FOURTEENTH EUROPEAN ROTORCRAFT FORUM

Paper No. 110

ESTIMATION OF ROTOR BLADE INCIDENCE AND BLADE DEFORMATION FROM THE MEASUREMENT OF PRESSURES AND STRAINS IN FLIGHT

John Riley
Gareth Padfield
Jane Smith

Flight Dynamics Division
Royal Aerospace Establishment
Bedford, MK41 6AE England

20-23 September, 1988
MILANO, ITALY

ASSOCIAZIONE INDUSTRIE AEROSPAZIALI
ASSOCIAZIONE ITALIANA DI AERONAUTICA ED ASTRONAUTICA

SUMMARY

Current research at the Royal Aerospace Establishment UK is directed towards the development of advanced control systems for helicopters. Measurements of rotor loading distributions in manoeuvring flight are being made at RAE to facilitate this aim. A special technique for deriving local incidence from a single pressure measurement has been developed. This paper describes the background to this research and presents preliminary results.

1 INTRODUCTION

Current work at the Royal Aerospace Establishment, UK, includes a long term research programme to enable advanced control systems to be developed for helicopters. This necessitates the development of improved mathematical models capable of representing the helicopter rotor system not only in steady trimmed flight, but also during transient manoeuvres. In particular, improved models are required to improve the piloted simulation studies, which form an important part of the research programme on helicopter agility.

Measurements of the aerodynamic loadings generated on rotor blades in flight are required to support this research. These measurements may be used to validate existing modelling techniques or, more usually, indicate the limits of their validity and by defining the discrepancies, guide the development of improved models. The complexity of the aerodynamic loading distribution on the rotor poses a formidable measurement problem; earlier flight research at RAE[3] has highlighted the difficulties of making an accurate determination of local lift on the blade by integration of pressures measured around the chordline. However, in the course of this flight research, it has become almost standard practice to use the magnitude of a single pressure measured on the upper surface of the blade near the leading edge as a measure of the local normal force coefficient. Similarly, the pressure measured near the trailing edge, by its abrupt reduction when flow separation occurs, has been found to be a good indicator of the onset of blade stall.

This paper gives an account of how this earlier, mainly qualitative, use of such "incidence indicator" and "stall indicator" sensors is currently being extended to provide automatic displays of rotor incidence and lift distributions, including the definition of stalled areas of the rotor disc. Where previously the incidence indicator sensors were used mainly to define major loading features such as vortex interactions, the current analysis has been developed, using data from oscillatory aerofoil tests in a wind tunnel to derive values of incidence and lift coefficient of acceptable accuracy. As for the stall indicator sensors, where in the earlier work the onset of separation was assessed by eye from examination of selected trailing edge pressure time histories, the analysis has now been developed to automatically detect stall by the application of a "threshold" criteria to this pressure measurement.

The Puma helicopter used for this flight research (Fig 1) is equipped with a digital magnetic tape airborne recording system. In addition to an array of 'indicator sensors' as described above, blade strain measurements, and rotor blade and aircraft motions are

recorded. By simultaneously measuring the blade elastic deformations and the local aerodynamic incidence on the blade, the constituent parts, which include in-flow angle, blade elastic twist, blade elastic flap induced incidence and rigid blade flap induced incidence can be deduced. This breakdown can then serve as a guide to the level of refinement needed for the various elements of the modelling, such as the wake representation and the blade dynamic model. The use of an individual indicator sensor instead of the entire chordwise pressure distribution leads to a large reduction in the number of parameters to be recorded. The full capacity of the airborne recording system can then provide a very high sample rate on each channel, and gives the capability to record continuously the entire rotor loading and strain distributions throughout transient manoeuvres.

Examples of some preliminary results from the current tests are given in the paper which show the variation of measured loadings with air speed in level flight, and also some comparisons with predictions are shown. It is recognised that the complexity of the flow on the rotor is not fully represented in the two dimensional oscillatory wind tunnel tests from which the correlation between the pressure near the leading edge and lift is derived. Clearly neither the rates of change of Mach number are present in the tunnel tests, nor the radial loading gradients generated by the proximity of blade tip vortices, with their associated effects on stall onset. Because of this, examples are shown comparing values of local lift measured on the rotor by integration around the chordline, with values derived from the indicator sensor. These additional measurements have proved to be valuable in assessing the accuracy with which lift can be derived from the indicator sensor in fully representative flight conditions. The actual test programme is in its early stages, but some assessment of the results obtained so far, and the proposed content of the overall manoeuvre loads programme will be given.

2 EXPERIMENTAL FACILITIES

The Puma helicopter used for these tests is the fully instrumented aircraft which has been used for flight research tasks at RAE Bedford UK for a number of years[1] (Fig 1). The on-board recording system is capable of recording all aircraft rates and attitudes, control positions and blade motions. In addition, for this work, a metal main rotor blade is equipped with arrays of strain gauges and pressure sensors to determine the blade deformations and aerodynamic loads.

The pressure sensors, as discussed in the Introduction, are positioned to give an indication of local blade incidence, and also to detect blade stall. Detail of the interpretation of these sensor outputs is given in section 3. The principle employed is that simple pressure measurements made in flight can be related to extensive wind tunnel pressure measurements made on the same aerofoil section. Hence that elusive quantity - local blade incidence can be derived.

The blade sensors, gauges and wiring are all applied externally on the blade surface to maintain the integrity of the blade structure. to make this possible, whilst causing only neglible disturbances to the profile, miniature 'Kulite' semiconductor pressure sensors are installed as shown in Fig 2. The sensor on the upper surface at 2%

chord can be accommodated by making a small, smooth recess in the blade spar. The dimensions of this recess are within the normal blade damage repair limits, so no further reduction of the normal fatigue life is caused. Similarly, for the "stall indicator" sensor at 98% chord the externally mounted sensor is locally blended into the surface by a fairing, the flow in this region not being so sensitive to minor changes in the local shape. Wiring connections to the hub-mounted amplifiers are in a thin loom on the lower surface, blended in to the rear of the normal anti-erosion strip. Small blade balance adjustments are made by changes to the blade tip balance weights, so that, overall, the instrumented blade can be considered identical both aerodynamically and dynamically, to a standard Puma blade.

An array of such sensors, 17 near the leading edge and 9 near the trailing edge is located as in Fig 3. The location of the strain gauges enables measurement of flap and lag bending moments and blade torsion at the radial positions shown by the abbreviations 'F' , 'L' and 'T' in Fig 3. Their radial positions have been chosen so that the measurements define most accurately the important flap lag and torsion modes of vibration of the blade as discussed in section 3.

The main on-board recording system uses a digital magnetic tape recorder and the elements of this system are outlined in Fig 4. Blade sensor and gauge measurements are amplified on the rotor head before being transmitted by slip rings to a multiplexer which feeds the data in serial form onto the recorder. The Central Processor permits a choice of the sampling rate which can be chosen for each channel within a limit of 128 K samples/sec total. Priority has been given to the pressure and strain measurements to give a good definition of these quantities (1024 samples/sec). Care has been taken to ensure that 'Skewness' errors do not affect the unsteady airloads and blade vibration analysis. In addition to the on-board recording, a telemetry system is used to transmit selected strain measurements from the blade and control system to a ground station for real-time monitoring during the flight. This is an important part of the data acquisition system since it enables fatigue damage accounting and the observation of maximum load limits. This permits the helicopter to be safely operated outside the normal Service release.

Regular calibration of the pressure sensors on the blade has been found to be an essential part of such flight tests if accurate results are to be achieved. A linear characteristic is used to define the sensor output. Zero checks are performed automatically before and after each flight and at frequent intervals during the progress of the trial a check of the sensitivity of each sensor is made. This is conveniently achieved by inserting the blade into a pressure chamber (Fig 5). Thus with the blade still connected to the helicopter's recording system, pressure changes corresponding to the working range of the sensors can be applied by pressurisation, or evacuation of the test chamber.

3 ANALYSIS TECHNIQUES TO INTERPRET MEASUREMENTS

3.1 DERIVATION OF INCIDENCE AND SEPARATION

Leading edge pressures have been used in previous flight experiments[1] at RAE to indicate incidence, α , and normal force

coefficient, C_N , in a mainly qualitative way. An example of the correlation between C_N and leading edge pressure coefficient is given in Fig 6. The close correlation even during blade vortex interaction at azimuth 90° and 270° is readily apparent. The technique stems from the observation of a near linear relationship, in static conditions, between the upper surface pressure coefficient near the leading edge and C_N as evidenced in two-dimensional tunnel tests. The position of 2% chord was chosen to minimise structural weakening of the Puma blade resulting from the small depression in the blade spar necessary to accommodate the transducer into the profile. Other positions in the range 0-3% c would in general be suitable from aerodynamic considerations but with various non-linearities (as is the case at 2% c) principally from effects due to the compressibility of the flow.

The sudden change in upper surface trailing edge pressure coefficient (trailing edge pressure divergence) at flow separation and stall has been used as a stall indicator. Fig 7a&b, taken, from Ref 1, illustrate leading and trailing edge pressure coefficients (C_{p02} , C_{p98}) during attached and separated flow during unsteady two-dimensional wind tunnel tests. Apart from demonstrating the above mentioned features, two others are apparent: the small but not insignificant hysteresis in attached flow and the very pronounced hysteresis between separation and re-attachment when separation is present.

In broad outline, using the leading edge data, local incidence and normal force coefficient are calculated allowing for the variation of section characteristics with Mach Number (M) and with compensation for unsteady incidence effects (at constant M) during attached flow only. Points marking the onset of flow separation and re-attachment are detected and marked and estimates of C_N and α in separated flow regions suspended. The various stages are briefly described below and where applicable, left in the program as options so that the magnitude of the various contributions can be assessed.

1) The static section data (Fig 8a&b) are given in terms of C_N versus C_{p02} and C_N versus α . They form part of the static "look-up" table. They refer to transition fixed tests but a similar set is encoded for transition free conditions as a second option. The difference, except near $C_{N_{Max}}$ is relatively small. The curves for each Mach number are extended as shown by the dashed lines, to improve interpolation procedures. If the static $C_{N_{Max}}$ is exceeded, this is identified during the the subsequent calculation.

2) In correcting static values of C_N and α derived from C_{p02} for unsteady effects two distinct processes are involved.

a. The derivation of C_N from C_{p02} .

b. The derivation of α from C_N .

Hence separate C_N versus C_{p02} , and α versus C_N , relationships are required. Based on unsteady two-dimensional

tunnel tests, Beddoes[2] observed that the phase lag of leading edge pressure with C_N was linear with reduced frequency giving a relationship of the form :

$$C_N = C_N' \, (1 + T_p \, \dot{C}_p) \qquad 1$$

where C'_N is the static value and T_p is suitably chosen time constant.

The basis of the method[2] for obtaining α from C_N rests on the assumption that C_N corresponds to the "static" value obtained from the look-up table unless α has changed in the recent past. If α has increased, then the static value lags the actual value by an amount dependent on the magnitude of the change and how recent its occurrence. The corresponding deficit in α to that read directly from the look-up table takes the form:

$$\Delta\alpha' = \Delta\alpha \, (A_1 e^{\frac{-t}{T_1}} + A_2 e^{\frac{-t}{T_2}}) \, (1-M^2)^{0.5} \qquad 2$$

where

α is the actual incidence

α' is the static value

A_1 , A_2 are constants

T_1 , T_2 are time constants dependent on the local chordwise velocity and M , is the local Mach number.

The total deficit in α' resulting from the time history of the recent past is described by a gate on n (say 10) equations based on the expression given above at $(n - 1)$ past intervals which, solved sequentially, enable the true value of α to be determined. The gate moves progressively through the 230 (nominal) data points per revolution of the blade and this process is implemented at each leading edge measurement station.

3) Two options are available to determine the point in azimuth at which separation and trailing edge pressure divergence, if present, occurs. One depends on detecting a sudden change in level of C_{p98} in a negative sense. An average of some 3 successive points is used to reduce the effects of spurious noise in the data. The other examines the slope of the best line through 5 successive points and compares it with the previous 5. The number used is selectable and the point of maximum difference in slope is the point of separation.

Any constant error in pressure arising from zero or gain errors of the pressure sensors, or error in ambient pressure

determination when divided by the local dynamic pressure, causes the coefficient to vary with azimuth and can mask trailing edge pressure divergence should it occur. The effect is magnified at inboard regions of the retreating blade where the dynamic head becomes relatively small causing the trailing edge pressure coefficient to rise steeply showing an apparent but spurious separation. This can be avoided by exercising an option to re-calculate the pressure coefficients having added a constant value to the measured static pressure, calculated to make the trailing edge pressure coefficient the same value at azimuth 90° and 180° where separation is absent, a condition which is essentially true in attached flow.

Re-attachment occurs when C_{p98} returns to a pre-selectable value. The program is undergoing continous development as various features in the results become apparent.

3.2 VALIDATION USING DIRECT MEASUREMENTS OF LIFT ON A ROTOR BLADE

The results from surface pressure measurements at the rectangular tip of a gloved Puma blade made during tests to compare with a tip of similar area but swept planform have been used in the present validation[3]. The values of C_N obtained from the 23 upper and lower pressures at 95% radius are compared with that estimated from the leading edge pressure coefficient only in Fig 9.

Before making comparisons, the actual blade profile needs to be discussed. The front part of the section was defined by a NACA 0012 thickness distribution based on a chordline of 82% of the actual overall chord. The rear part was similarly defined and the two parts joined by a blend line in the region of maximum thickness to give a resulting thickness/chord ratio of 10%. The data from the NACA 0012 look-up tables was subsequently adjusted using calculated pressure distributions for NACA 0009 and NACA 0012 profiles. The leading edge sensor was still at 2% of the overall chord and the adjustments made must by their nature be considered approximate.

There is no separated flow in the particular level flight condition shown in Fig 9 and the effects of blade vortex interaction on C_N values derived by integration and from C_{p02} at azimuth 90° and 270° are in agreement but in general the C_{p02} values are higher than the integrated values in the first and final quadrants of azimuth. These differences are apparent in other flight conditions in this series of tests.

The values of C_N determined from C_{p02} are derived from steady section data only, ie they have not had the phase lead described previously applied. There does not appear to be an obvious case for the application of a lead on the static values at this flight condition.

Considering the 'once-per-rev' rates of change of incidence, application of the required phase lead would reduce the apparent discrepancy between 330° and 70° azimuth, but would introduce larger discrepancies between 120° and 270°, achieving no better overall agreement. Also the effect at the higher frequencies would be to increase the amplitude of the local peaks relative to the integrated

values which are more or less in agreement when uncorrected. Also, regarding unsteady effects, flight tests at RAE[5] indicate a partial cancellation of unsteady incidence effects by unsteady Mach number effects, an aspect receiving consideration in the current work.

A further factor concerning the limits of validity of the incidence correlation is the degree of three-dimensionality of the flow because of proximity to the tip (95% R). Previous tests[4] in the tip region show the presence of forward loading, an effect which if present would overestimate C_N determined from C_{p02}. Three dimensional flow effects are also expected during close blade vortex interactions. In these respects an analysis of previous tests using a gloved section (not NACA 0012) inboard at 0.8 R showed a much closer agreement with integrated values of C_N.

Overall the comparisons made indicate that when applied to the Puma blade, which is much closer to a NACA 0012 section, the resulting C_N values will lie much closer to those which could be obtained by extensive integration. The application of the appropriate lead to the static C_N needs further consideration and is partly dependent on the necessary accuracy required in association with the other measurements, in this analysis of rotor loading distribution particularly the accuracy of incidence obtained from blade elastic deformations. The application of the exponential time delays to correct the static values of local incidence and obtain the actual incidence time history are still required and here again the error involved, if the correction is not applied, will depend on the nature of the existing incidence time history.

An example of the definition of the point of separated flow and re-attachment is given in Fig 10. Again it is taken from tests on the rectangular tip described previously in a flight condition with retreating blade stall. In this particular case, both methods, one using a change in general level and the other a change in slope of C_{p98} define the azimuth angle of separation onset with acceptable accuracy. Difficulties may arise if separation is incipient and of short duration.

3.3 DERIVATION OF BLADE DEFORMATION

Rotor blade displacement relative to a hub-fixed coordinate system can be expressed in terms of flap, lag and torsional motions. Subscripts r and e define the rigid blade and elastic components respectively. The rigid blade twist angle is made up of two components, one from the pitch angle applied through the control system (Θ_p) and the other from the built-in twist of the blade (θ_{tw})

$$\Theta_r = \Theta_p + \Theta_{tw} \quad . \qquad 3$$

The control system input Θ_p modified by the elastic response of the control system to the blade torsional vibrations, is measured on the Puma by a sensor on the pitch bearing; the blade static twist angle varies linearly by 8° from the shaft axis to the blade tip. Pitch angle changes due to elastic torsion are derived from the strain gauge measurements as discussed below. Blade flap angle is similarly composed of elastic and rigid components, and like torsion, both contribute to a rotation at the bearing. The elastic component first

needs to be derived before the rigid blade flap angle can be deduced. The derivation of blade elastic flap displacement and torsional angle is achieved using the technique of strain pattern analysis formulated at RAE[6]. In the SPA technique a series of calibration modes are used with known relationships between blade shape and the corresponding strain or bending moment distribution. In previous RAE studies the calibration modes have been based on non-rotating coupled modes and the required strain/displacement relationship derived from experiment. In the case where the structural properties of the blade are well known, theoretical in-vacuo modes could serve equally well. The strain pattern measured in flight is then represented as a linear combination of calibration mode patterns and the blade displacements reconstituted using the known transformation matrix giving a least squares match.

For the Puma blade shown in Fig 3, the limited number of strain gauge locations imply the use of a limited number of calibration modes to avoid under-determination. The calibration modes used are based on laboratory tests conducted on an extensively instrumented Puma blade (Ref 6), but with the strain/displacement relationships limited to the pattern in Fig 3. The calibration modes used, described in more detail in Reference 6, are the first four non-rotating coupled elastic modes; modes 1 and 2 dominated by flap, mode 3 by lag and mode 4 by torsion. The software package SPA has been integrated into a more comprehensive analysis package RIBAN (Research Instrumented Blade Analysis) describe below in section 3.4, outputting approximate blade flap and lag deflections and torsional angle for use in the computation of local blade incidence.

3.4 RIBAN - RESEARCH INSTRUMENTED BLADE ANALYSIS

An important feature of the software required for this type of research is that it enables the substantial amounts of data gathered to be handled efficiently and relatively easily by users with differing levels of computing expertise. To this end a number of FORTRAN programs have been written and incorporated with existing software available in Flight Management Department (FMD), Bedford, into a 'user friendly', menu driven package RIBAN. The constituent parts that make up the RIBAN package are described below and briefly outlined in Fig 11.

3.4.1 MANS - MODAS ANALYSIS SYSTEM

A set of software tools has been developed for FMD[7] to aid in handling and analysing trials data gathered on a Plessey High Density MODAS (Modular Data Acquisition System), a system widely used throughout the UK Ministry of Defence. As an element of these tools, MANS (Modas ANalysis System) takes the form of three individual programs CONTAP, EXTRACT and TIMEDIT, the collective aim of which is to read computer compatible tapes (CCT) produced by the MODAS ground replay Facility into the FMD VAX computer. CONTAP reads one or many data sequences from the CCT and transfers them to disk files, reorganising the data slightly to ease further processing by the EXTRACT program. The EXTRACT program can then be run to read and calibrate user selected data and place them into separate files of time series data for each measured parameter. These files are in a form compatible with the Data Analysis Terminal System (DATS) described below.

If data for a single turn of the rotor only is to be selected for analysis, an interactive program TIMEDIT, provided as part of the MANS software, can be run to allow selection and editing of EXTRACTed parameters to form new runs.

3.4.2 DATS - DATA ANALYSIS TERMINAL SYSTEM

DATS[8] is a collection of modules for the analysis and display of time series data. Each module is an individual program designed to perform a single function. Several modules can be grouped together by the user into 'jobs' which can also include FORTRAN code. DATS also incorporates numerous subroutines to enable users to create their own modules to supplement those already provided. Such modules make up the major part of the analysis the RIBAN package performs. For example, density correction of parameters, main rotor blade pressure normalisation and incidence estimation. Standard two and three dimensional data displays of these parameters are provided in DATS 'jobs' but the user is also free to perform his own data displays and analyses outside RIBAN but within DATS.

3.4.3 SPA - STRAIN PATTERN ANALYSIS

The SPA software[6], referred to in section 3.3, reads calibrated files of blade flap and lag bending moment and blade torsion (from strain data) and blade root pitch, flap and lag angles. Graphical output from SPA includes calibration mode shapes and strain patterns, reconstructed blade deflections and fit-error functions. Data output files are created for blade deflections and velocities for use in the incidence/downwash computation module.

3.4.4 INCIDENCE/DOWNWASH COMPUTATION

Local blade chordline incidence as a function of radius and azimuth can be expressed as a combination of two principal effects - the orientation of the blade chordline with respect to the hub axes (θ) and the inclination of the local velocity component to the path of the local blade element (ϕ) (See Fig 12 & 13)

$$\alpha\ (r,\ \psi) = \theta + \phi \qquad 4$$

where

$$\theta = \theta_p\ (\psi) + \theta_{tw}\ (r) + \theta_e\ (r,\ \psi) \qquad 5$$

$$\phi = \phi\lambda\ (r,\ \psi) + \phi\beta_r\ (r,\ \psi) + \phi\beta_e\ (r,\ \psi) \qquad 6$$

where θ_p is the blade pitch input from the control system, θ_{tw} the built-in twist and θ_e the elastic torsion (output from SPA). The inflow ϕ is made up of three components,

$$\phi\lambda = \frac{(\mu_z - \lambda) + r\omega_y}{U_T} \qquad 7$$

$$\phi_{\beta r} = \frac{-\beta_r (\mu_x \cos\psi - \mu_y \sin\psi) - r\beta'_r}{U_T} \qquad 8$$

$$\phi_{\beta e} = \frac{-\beta_e (\mu_x \cos\psi - \mu_y \sin\psi) - r\beta'_e}{U_T} \qquad 9$$

and

$$U_T = r(1 + \omega_x \beta) + \mu_x \sin\psi + \mu_y \cos\psi \qquad 10$$

$$\omega_x = \frac{p}{\Omega} \cos\psi - \frac{q}{\Omega} \sin\psi \qquad 11$$

$$\omega_y = \frac{p}{\Omega} \sin\psi + \frac{q}{\Omega} \cos\psi \qquad 12$$

μ_x, μ_y and μ_z are the normalised (by ΩR) velocity components at the rotor hub, λ the normalised inflow, r the normalised (by R) rotor radius; β_r and β_e the local rigid and elastic components of blade flap, β (See Fig 13). A prime denotes differentiation with respect to azimuth angle ψ, Ω is the rotor speed and p and q the hub pitch and roll rates.

4 FLIGHT MEASUREMENTS AND LOADING PREDICTIONS

Although this work is in its early stages, some examples from the small proportion of the planned flight tests completed so far are of interest. They illustrate both the aerodynamic loadings and the kind of blade dynamic responses measured. Some preliminary comparisons of these measurements with loading predictions are also included.

Contour plots of the measured incidence distribution over the rotor disc provide a convenient way to illustrate the overall definition of the main loading features provided by the 'indicator' sensors. Fig 14 shows the development of the loading patterns in level flight for a range of airspeeds. The 'Hover' condition is mainly axisymmetric with a progressive increase in incidence towards the tip. Possibly due to small, unintentional, translational velocity, loading perturbations are apparent in the third quadrant due to an inward displacement of the tip vortices on this side of the disc. At 48 kn the lateral imbalance of incidence due to forward speed already begins to appear and the distinct loading peak at around 0.8 radius shows at the front of the disc. This is clearly a result of the interaction with the wake of the previous blade. As speed increases, the advancing side of the disc, as expected, moves progressively towards lower incidence levels free from any significant wake interactions and hence varying only slowly with radius and azimuth. On the retreating side the wake interactions assume greater significance. At a speed of 141 kn, in the third quadrant, the higher incidences can be seen to progress out along the blade as 270° azimuth is approached. At even higher thrust levels than shown in this example, these high incidence regions become the stalled areas on the retreating blade

side, although it must be admitted that the loading patterns become more complex at higher thrust levels as blade dynamic distortions begin to modify incidence levels more significantly.

Some indication of the relative magnitude of the rigid blade displacements and the blade elastic deformations for these same flight conditions is shown in Fig 15. These plots show the flap displacements and deformations derived from the strain gauge and blade root angle measurements. The fluctuating part is mainly of interest here. At each of the speeds shown, note that even the rigid blade flap has significant higher harmonic content. In addition, the fluctuating elastic flap distortions are of comparable amplitude, and of course have significant high frequency content too. These measurements show the need for detailed blade dynamic models if loading distributions are to be accurately predicted.

Finally a comparison of measured values of lift with results from two load prediction programs in current use at RAE is shown in Fig 16. These lift values are at 0.95 radius on the blade, and for the purpose of this comparison it is sufficiently accurate to compare measured values of C_N (normal force coefficient) with C_L (lift coefficient). The solid line shows C_N derived by integration of the pressures measured around the chordline in flight, and the dashed line the corresponding value from the single indicator sensor, as described in section 3. For comparison with these measurements values of C_L from a 'ROTORLOAD' calculation (which uses a vortex ring model to represent the rotor wake, and a full modal calculation to find blade deformations) are shown by the dotted line. Also shown, plotted as discrete points, are results from 'HELISTAB' a much simpler "rigid blade uniform inflow" model used for piloted simulation work. Clearly, neither prediction matches the measured lift exactly, but Fig 16 gives some indication of the magnitude of the errors resulting at each azimuth angle. The need for a realistic representation of the wake interactions is clear from this example.

It is important to recognise that although in this paper, sample results are shown consisting of measurements made during only one turn of the rotor, the capability exists to record continuously at this same data rate. This is necessary of course to capture rotor loadings in transient manoeuvres, but it also allows the question of rev-to-rev repeatability to be addressed in steady trimmed flight. This is being done, to assess the validity of results measured in somewhat turbulent air conditions, and for the quite unsteady loadings experienced when extensive blade stall is present. For flight conditions such as those shown in this paper, averaging over many revolutions makes little difference to the results.

5 DISCUSSION AND CONCLUSIONS

Analysis of the first series of these flight tests is very much in its initial stages and so far only a limited range of level flight data has been examined. The planned flight programme will progressively cover the measurement of 'helicopter manoeuvre loadings' by measuring rotor loads in a series of flight conditions of increasing complexity. Having established a basis of steady trimmed flight conditions the tests are proceeding to include discrete control inputs, followed by a series of specific manoeuvres, and loadings measured in

designated 'agility tasks'. Also to be included are tests where rotor speed is varied to investigate rotor dynamic behaviour directly.

Values of lift and incidence determined from leading edge pressure are considered generally satisfactory, and are in reasonable agreement with predicted values, although the unsteady incidence corrections available are not included in the results presented.

Using data from a previous experiment on an instrumented blade tip, a preliminary application of a 'lead' to the C_N value read directly from the static relationship between C_N and C_{P02}, to correct for unsteady effects does not always appear to improve the correlation with C_N obtained by chordwise integration. The proximity of this particular test section to the tip, together with unsteady Mach number effects are possible factors to consider. In certain circumstances, the unsteady Mach number effects appear to partially cancel the effects of unsteady incidence. A detailed study of all the unsteady corrections proposed is presently in progress.

The blade deformations obtained from strain measurements using the SPA technique have also presented anomalies. There are uncertainties in the strain calibration pattern presently used. This arises because the pattern has been derived indirectly from calibration measurements on a different blade to that used in the present tests, and some doubt exists on the accuracy of the transfer of data to the present blade. This blade is shortly to be re-calibrated.

In emphasising some of the problems that have arisen, this in no way detracts from the potential of the techniques used to provide data of sufficient accuracy to guide the development of improved helicopter rotor mathematical modelling. In particular, as the analysis progresses, these simultaneous measurements of blade incidence and blade deformation will be used to make it clear how much wake interactions and blade dynamic response each contribute to the overall rotor loading distribution.

ACKNOWLEDGEMENT

The authors would like to thank Phil Brotherhood for his work on the analysis to derive incidence and separation on the rotor blades from the output of the indicator sensors. Without his valuable assistance this paper could not have been prepared. Thanks also to Peter Tarttelin who produced the loading and incidence results.

REFERENCES

1. P. Brotherhood: "An appraisal of rotor blade - tip vortex interaction and wake geometry from flight measurements" AGARD CP 334 1982.

2. T.S. Beddoes: "Representation of aerofoil behaviour" Vertica Vol 7 No 2 1983.

3. M.J. Riley and Judith V Miller: "Pressure distributions on a helicopter swept tip from flight tests and from calculations" presented at the IX European Rotocraft Forum, Paper No 9, September 1983.

REFERENCES (concluded)

4. M.J. Riley and P. Brotherhood: "Comparative performance measurements of two helicopter blade profiles in hovering flight" ARC R & M No 3792 1977.

5. P.G. Wilby, M.J. Riley and Judith V Miller: "Some unsteady aerodynamic effects on helicopter rotors" presented at the VII European Rotorcraft Forum, Paper No 47, September 1981.

6. A.R. Walker and D.B. Payen: "Experimental applications of strain pattern analysis (SPA) - wind tunnel and flight test results" presented at the XII European Rotorcraft Forum, Paper No 79, September 1986.

7. C. Jewel: "Operating guide for MODAS analysis system" Prosig Computer Consultants Ltd (1986).

8. "DATS user manual" Prosig Computer Consultants Ltd.

Copyright © Controller HMSO London 1988

Fig 1 RAE Bedford research Puma helicopter

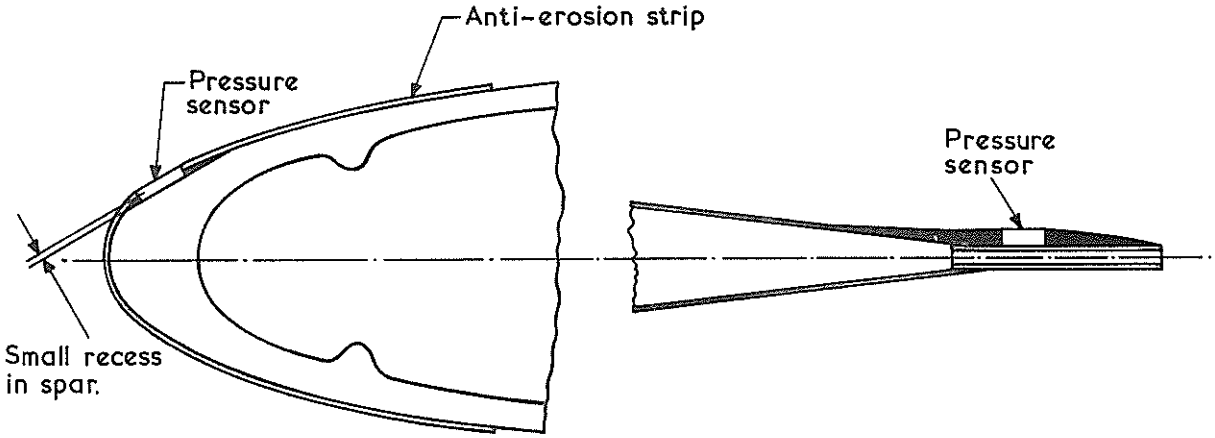

Fig 2 Location of indicator sensors near leading and trailing edges of blade

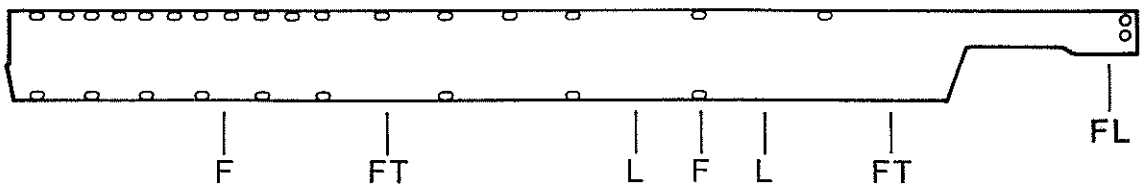

Fig 3 Distribution of strain gauges and pressure sensors along blade

Fig 5 Test chamber for pressure sensor calibration

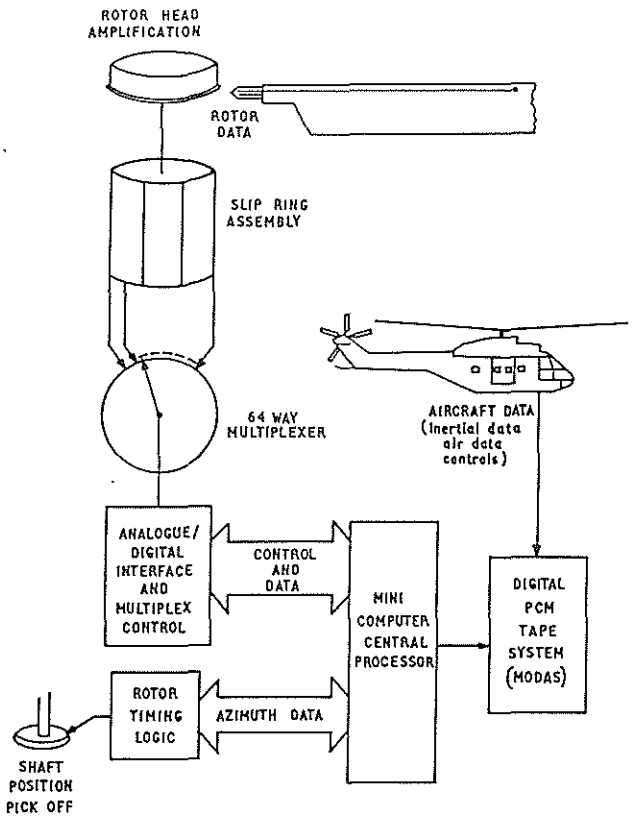

Fig 4 Schematic of data acquisition on research Puma

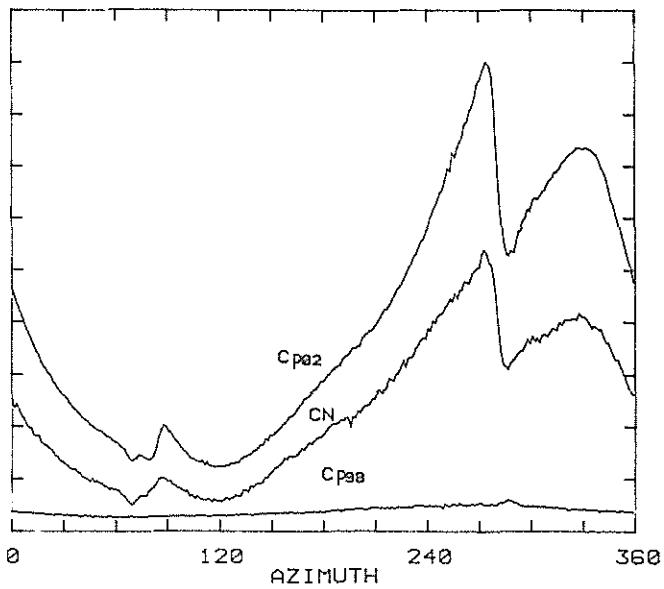

Fig 6 Correspondence between lift and the leading and trailing edge pressures

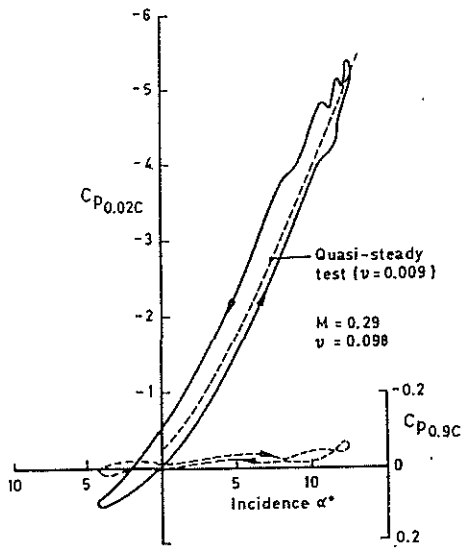

Fig 7(a) Leading and trailing edge pressure coefficients in attached flow

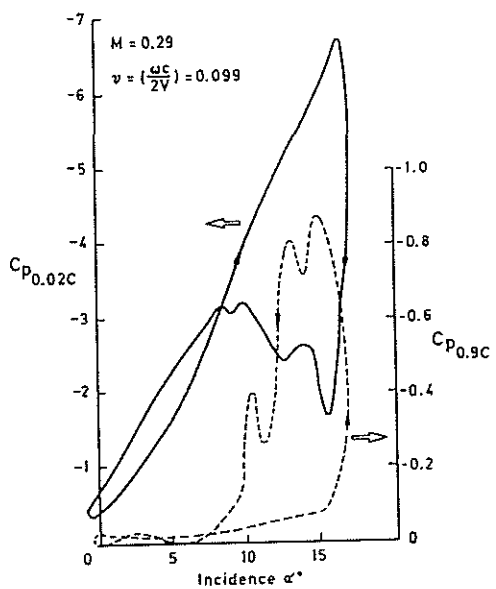

Fig 7(b) Leading and trailing edge pressure coefficients with separated flow

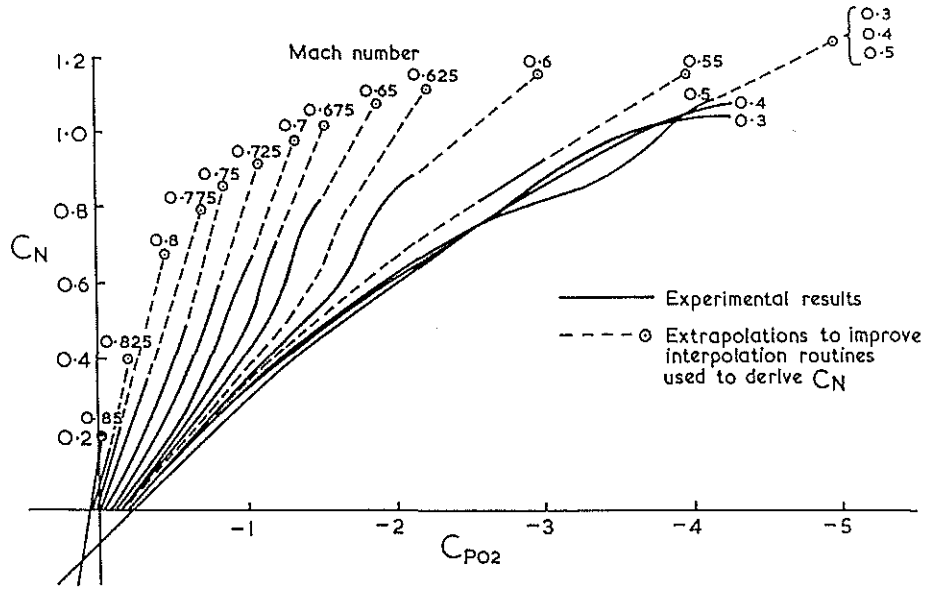

Fig 8(a) Correlation between lift and upper surface pressure at 2% chord derived from steady wind tunnel tests of NACA 0012 profile

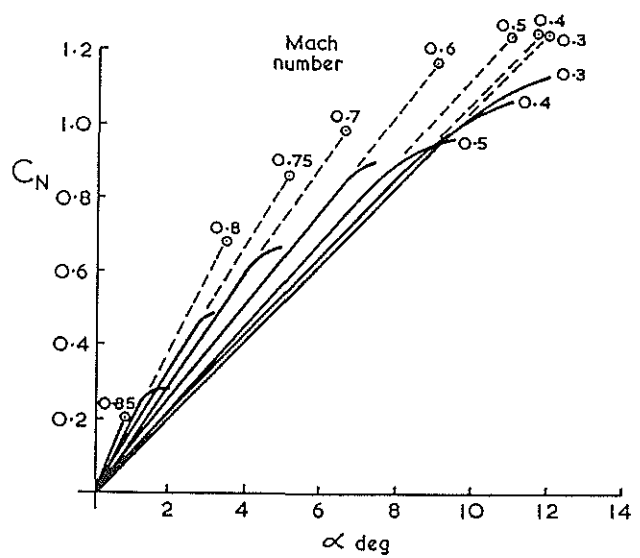

Fig 8(b) Correlation between lift and incidence derived from steady wind tunnel tests of NACA 0012 profile

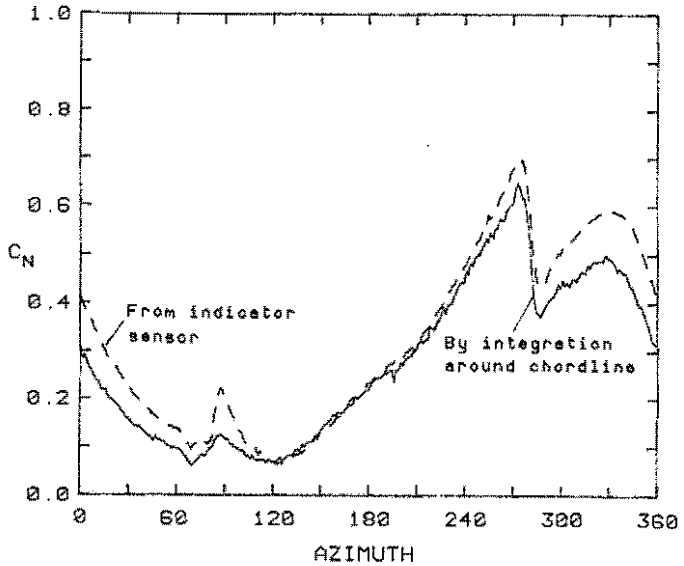

Fig 9 Lift derived from indicator sensor compared with lift by integration around chordline

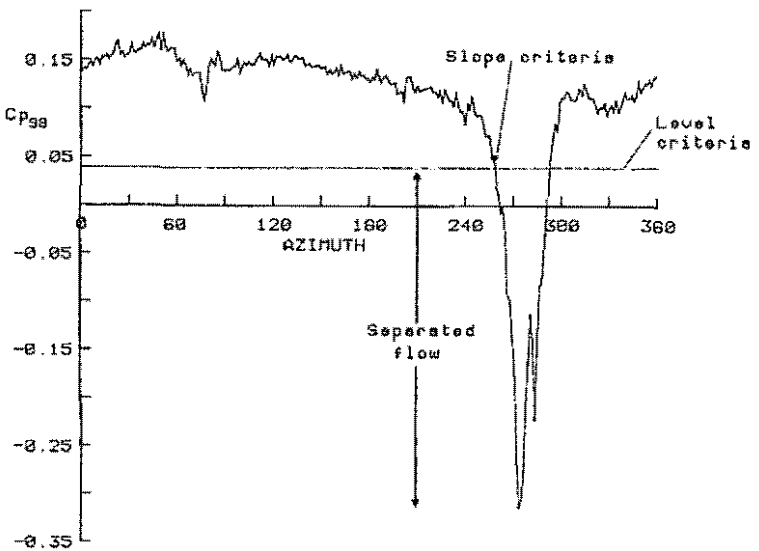

Fig 10 Stall derived from trailing edge pressure - 'slope' and 'level' criteria

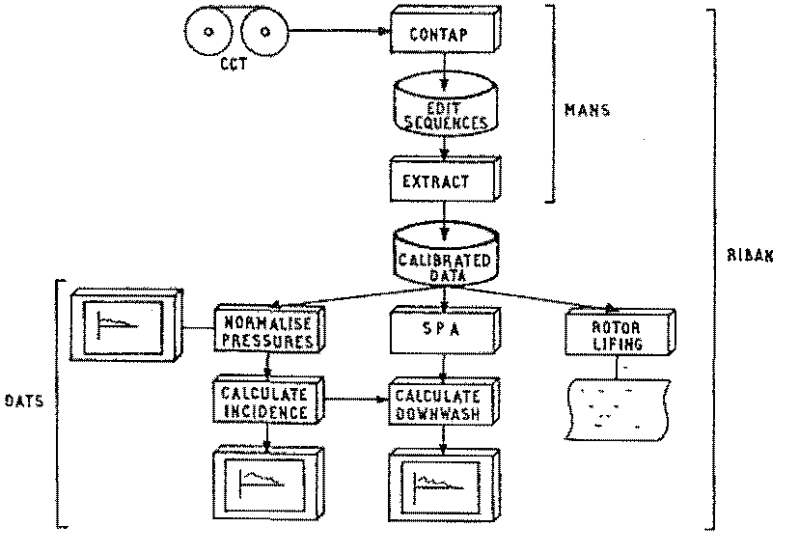

Fig 11 Elements of RIBAN package

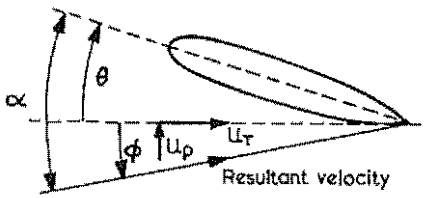

Fig 12 Blade section showing angles that make up total incidence

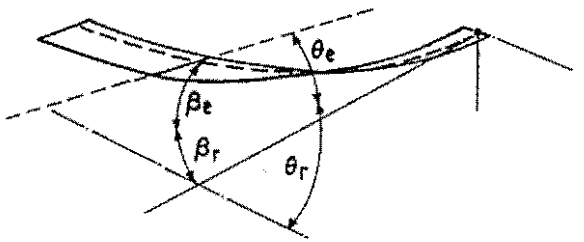

Fig 13 Blade displacements and distortions which determine blade element orientation

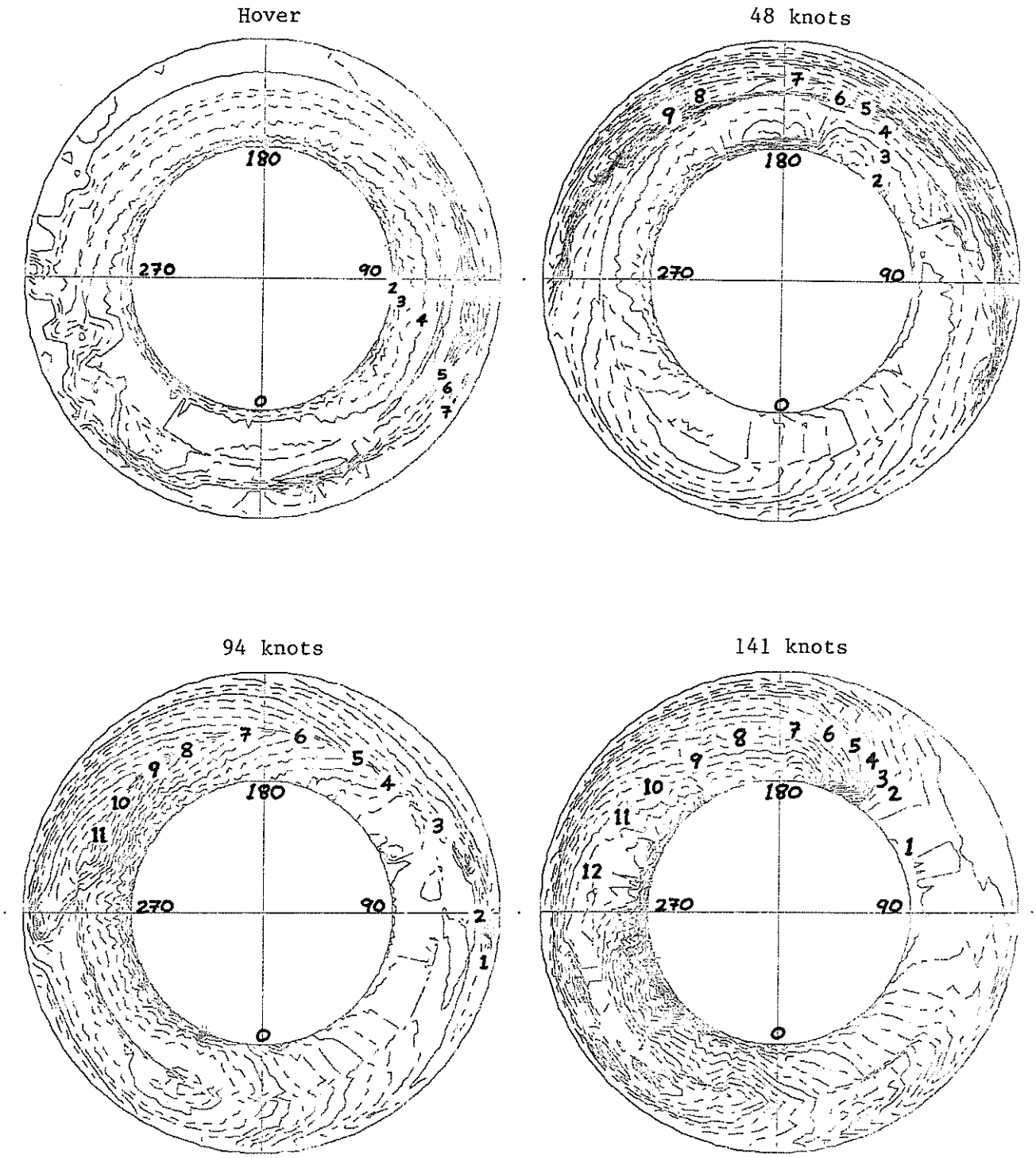

Fig 14 Blade incidence distributions measured for a range of speeds in level flight

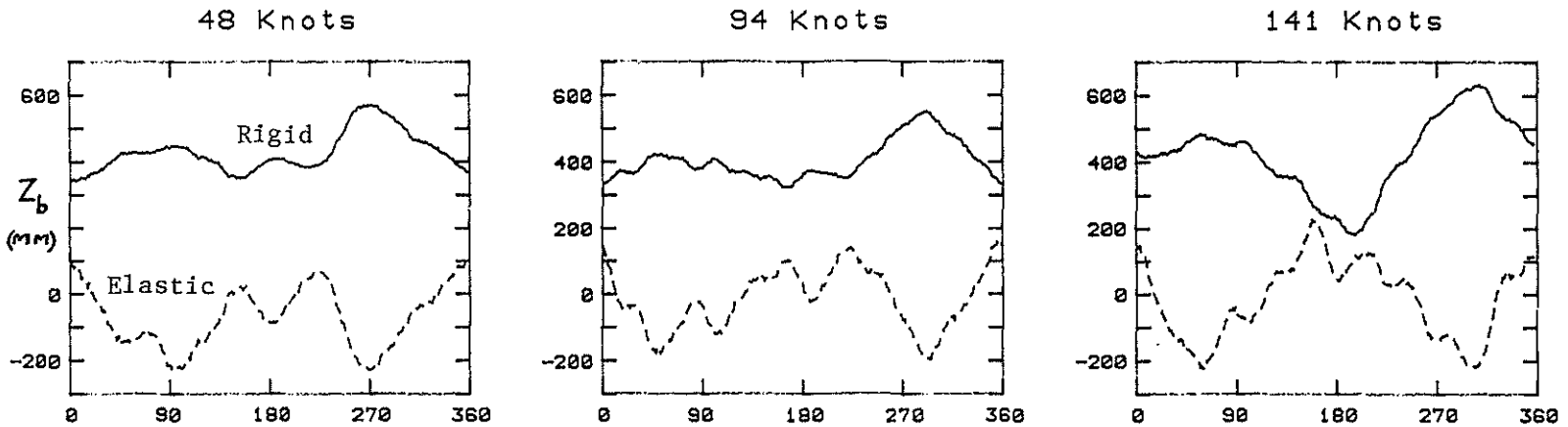

Fig 15 Rigid and elastic blade flap displacements at r/R = 0.75 in level flight

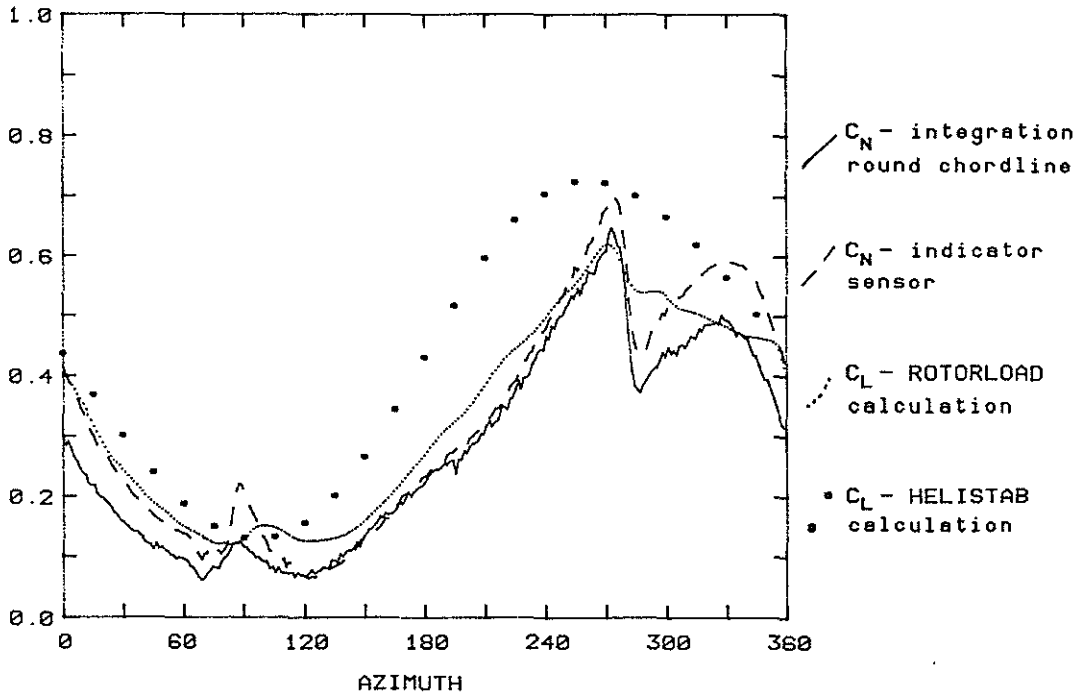

Fig 16 Comparison of measured and predicted values of blade lift